TWP-ICE global atmospheric model intercomparison: Convection responsiveness and resolution impact

Yanluan Lin,[1,2] L. J. Donner,[2] J. Petch,[3] P. Bechtold,[4] J. Boyle,[5] S. A. Klein,[5] T. Komori,[6] K. Wapler,[7] M. Willett,[3] X. Xie,[8] M. Zhao,[1,2] S. Xie,[5] S. A. McFarlane,[9] and C. Schumacher[10]

Received 14 October 2011; revised 23 March 2012; accepted 26 March 2012; published 8 May 2012.

[1] Results are presented from an intercomparison of atmospheric general circulation model (AGCM) simulations of tropical convection during the Tropical Warm Pool–International Cloud Experiment (TWP-ICE). The distinct cloud properties, precipitation, radiation, and vertical diabatic heating profiles associated with three different monsoon regimes (wet, dry, and break) from available observations are used to evaluate 9 AGCM forecasts initialized daily from realistic global analyses. All models captured well the evolution of large-scale circulation and thermodynamic fields, but cloud properties differed substantially among models. Compared with the relatively well simulated top-heavy heating structures during the wet and break period, most models had difficulty in depicting the bottom-heavy heating profiles associated with cumulus congestus during the dry period. The best performing models during this period were the ones whose convection scheme was most responsive to the free tropospheric humidity. Compared with the large impact of cloud and convective parameterizations on model cloud and precipitation characteristics, resolution has relatively minor impact on simulated cloud properties. However, one feature that was influenced by resolution in several models was the diurnal cycle of precipitation. Peaking at a different time from convective precipitation, large-scale precipitation generally increases in high resolution forecasts and modulates the total precipitation diurnal cycle. Overall, the study emphasizes the need for convection parameterizations that are more responsive to environmental conditions as well as the substantial diversity among large-scale cloud and precipitation schemes in current AGCMs. This experiment has demonstrated itself to be a very useful test bed for those developing cloud and convection schemes for AGCMs.

Citation: Lin, Y., et al. (2012), TWP-ICE global atmospheric model intercomparison: Convection responsiveness and resolution impact, *J. Geophys. Res.*, *117*, D09111, doi:10.1029/2011JD017018.

1. Introduction

[2] Our ability to accurately predict weather and climate is strongly influenced by the performance of the cloud and convection parameterization in general circulation models (GCMs) [*Randall et al.*, 2007]. In particular, a realistic representation of cloud and convective activity is critical to GCM performance in terms of its mean tropical circulation and tropical transient activities such as the Madden-Julian oscillation (MJO) [*Lin et al.*, 2006]. However, the ability of GCMs to predict these features involves the interaction of several subgrid parameterizations, such as the boundary layer, stratiform cloud, radiation, and convective parameterizations and this interaction poses an intriguing picture for understanding potential systematic biases.

[3] The Tropical Warm Pool-International Cloud Experiment (TWP-ICE) was conducted in January–February 2006 near Darwin, Australia with the aim to better understand tropical cloud systems and their associated anvil and cirrus microphysics and radiation [*May et al.*, 2008]. Comprehensive observations of large-scale flow and cloud measurements

[1]University Corporation for Atmospheric Research, Boulder, Colorado, USA.
[2]NOAA Geophysical Fluid Dynamics Laboratory, Princeton University, Princeton, New Jersey, USA.
[3]Met Office, Exeter, UK.
[4]European Center for Medium-Range Weather Forecasts, Reading, UK.
[5]Lawrence Livermore National Laboratory, Livermore, California, USA.
[6]Japan Meteorological Agency, Tokyo, Japan.
[7]Deutscher Wetterdienst, Offenbach, Germany.
[8]Institute of Atmospheric Physics, Beijing, China.
[9]Pacific Northwest National Laboratory, Richland, Washington, USA.
[10]Department of Atmospheric Sciences, Texas A&M University, College Station, Texas, USA.

Corresponding Author: Y. Lin, NOAA Geophysical Fluid Dynamics Laboratory, Princeton University, Forrestal Campus, PO Box 308, Princeton, NJ 08540, USA. (yanluan.lin@noaa.gov)

Copyright 2012 by the American Geophysical Union.
0148-0227/12/2011JD017018

provide a great opportunity for model evaluation and improvement. Distinct regimes (wet, dry, clear, and break periods) with a wealth of cloud and convective system types (shallow convection, locally forced thunderstorms, and organized oceanic mesoscale convective systems) at times associated with the propagation of the MJO over the Darwin region provide a useful test for models. To utilize the wealth of observations collected in the TWP-ICE, the U.S. Department of Energy Atmospheric Radiation Measurement program (ARM) [*Ackerman and Stokes*, 2003] and the Global Energy and Water-Cycle Experiment (GEWEX) Cloud Systems Study (GCSS) program organized a coordinated model intercomparison for TWP-ICE involving single column models (L. Davies, personal communication, 2011), cloud-resolving models [*Fridlind et al.*, 2012], limited area models (P. Zhu et al., A limited area model (LAM): Intercomparison study of the TWP-ICE case, submitted to *Journal of Geophysical Research*, 2012), and AGCMs. An overview of this multitype model intercomparison with its rationales is outlined (J. Petch, personal communication, 2011). This paper documents the results of the AGCM intercomparison for TWP-ICE as part of the coordinated effort.

[4] Evaluation of clouds and radiation in multiyear climate simulations using field experiment observations such as those taken during the TWP-ICE is difficult since the simulations represent only the long-term statistics of the atmospheric states. It has been recognized that many biases seen in AGCMs manifest themselves in the first few days of a model forecast started from analysis data. We follow the Cloud-Associated Parameterization Test bed (CAPT) approach, in which climate models are initialized with global analysis data for short-range weather forecasts and the resulting simulations are evaluated with field experiment measurements. This has been proved to be a valuable tool for model evaluation and improvement [*Phillips et al.*, 2004] because it provides a way to quantify model errors in a framework where the mean state of the atmosphere is close to observed. The CAPT approach has been applied successfully for Arctic clouds [*Xie et al.*, 2008], midlatitude cloud systems [*Williamson et al.*, 2005; *Boyle et al.*, 2005; *Williamson and Olson*, 2007], and tropical convective systems [*Petch et al.*, 2007; *Willett et al.*, 2008; *Boyle and Klein*, 2010]. The approach has also been regularly applied in some modeling centers to detect model systematic bias and guide model parametrization improvement [*Rodwell and Palmer*, 2007; *Martin et al.*, 2010]. Findings from these studies have detected model systematic biases and stimulated model improvement. For example, the detected upper-troposphere cold bias in Met Office Unified Model (MetUM) has been reduced by an adaptive detrainment parameterization for convection [*Derbyshire et al.*, 2011]. *Boyle et al.* [2008] showed some type of limiter in convective parameterization helped improve the MJO simulations via vertical heating structure change.

[5] Recently, the impact of horizontal resolution on AGCM simulations of tropical convection and precipitation was investigated. For example, using GFDL AM2, *Lau and Ploshay* [2009] found higher resolution simulations generally better resolved features such as topographical forcing and land sea contrast, whereas *Jung et al.* [2006] showed the need for mesoscale resolutions for a realistic representation of synoptic systems and associated eddy heat transport. However, time-mean precipitation errors, tropical model biases and variability generally only weakly depend on the resolution of the models [*Kim et al.*, 2011]. As shown by *Jung et al.* [2010] and *Boyle and Klein* [2010], model improvements in the Tropics depend critically on the physical parameterizations and the convection in particular. *Boyle and Klein* [2010] noted the gains in going to higher resolution were fairly moderate and some inherent errors in the model associated with physical parameterizations cannot be ameliorated with resolution only. To extend these resolution sensitivity studies, several models in this study are run at two different resolutions to investigate the resolution impact on tropical cloud and precipitation simulation with AGCMs.

[6] The objectives of the study are twofold. One is to document the relative performance of current global weather and climate models on different types of tropical convection given realistic initialization, with a focus on cloud properties and vertical diabatic heating structures. The other is to investigate how horizontal resolution impacts model cloud and precipitation characteristics, especially on the precipitation partitioning and precipitation diurnal cycle.

[7] Observational data and participating models are described in section 2. Section 3 compares model results with available observations and emphasizes the impact of model resolution. Key findings are briefly summarized in Section 4.

2. Observations, Model Description and Experiment Setup

[8] Observations used for model evaluation include the three hourly variational analysis by *Xie et al.* [2010], hourly convective and stratiform precipitation and their respective heating profiles from the C-band polarimetric (C-POL) radar [*Boyle and Klein*, 2010; *Fridlind et al.*, 2012], and various microphysical retrievals assembled and summarized in Cloud Retrieval Ensemble Data set (CRED) [*Zhao et al.*, 2012]. The variational analysis also provides the apparent heating and drying profiles (Q1 and Q2) [*Yanai et al.*, 1973] and includes surface and TOA radiation. TOA radiation was measured by the geostationary satellite MTSAT-1R and retrieved following *Minnis et al.* [2001], and surface radiation was recorded by radiometer measurements. Precipitation from the variational analysis is retrieved from the C-POL precipitation radar and represents an area with a radius of ~150 km surrounding Darwin. Cloud microphysical retrievals, especially for ice water content (IWC), have large uncertainties [*Protat et al.*, 2007; *Heymsfield et al.*, 2008]. CRED provides hourly average of 2 retrievals of liquid water content (LWC) and 5 retrievals of IWC based on the millimeter wave cloud radar (MMCR), micropulse lidar (MPL), and microwave radiometer measurements [*Zhao et al.*, 2012]. These retrievals are based on measurements at a single location. One LWC retrieval includes drizzle and rain and is generally larger than the other considering cloud droplets only. LWC retrieval is scaled by the liquid water path (LWP) measured by the microwave radiometer and more reliable at times having negligible precipitation contamination [*Turner et al.*, 2007]. The 5 IWC retrievals use different methods and assumptions about the ice particle properties [*Zhao et al.*, 2012] and thus give an estimate of the retrieval uncertainties. However, there are other sources of uncertainty not included in the above estimates. These sources include the fact that the radar calibration is not well known, the MMCR saturates in heavy

precipitation and so rainwater content and therefore attenuation may be under-corrected, no attenuation correction for the melting level is applied, and few in situ measurements of tropical cloud properties exist (especially in high IWC clouds). We also use Cloud Archive User Service (CLAUS) [*Yang and Slingo*, 2001] and the European Centre for Medium Range Weather Forecasts (ECMWF) analyses to describe the synoptic evolution. Finally, Tropical Rainfall Measuring Mission (TRMM) 3B42 precipitation [*Huffman et al.*, 2007] is used to describe the precipitation spatial distribution and temporal evolution over a large region near Darwin (Figures 2 and 8).

[9] A total of 9 models from 7 modeling centers (Table 1) participated in the intercomparison. Models include global operational weather prediction models (MetUM, IFS, GME, JMA) and climate models (MetUM, AM2, AM3, HIRAM, CAM4, and GAMIL). These models (except GME [*Wapler and Lane*, 2011]) were initialized at 00 UTC daily from the ECMWF operational analyses using the CAPT approach [*Phillips et al.*, 2004]. Wind, temperature, moisture, and surface pressure are initialized from the analyses, while other fields, such as land surface properties (vegetation, soil moisture and temperature), are ensured to be realistic from previous forecasts or spun-up simulations. Model second day forecasts, hour 24 to 45 every 3 h, are stitched together and used for the intercomparison. The Day 2 forecast is used to give each model enough time to adjust while maintaining a state close to the observed conditions. No nudging or other relaxation methods are applied to the forecasts. Five models have simulations at two horizontal resolutions with the highest resolution of ~20 km (Table 2). The intercomparison focuses on tropical cloud and convection simulations, which are significantly affected by the model stratiform cloud scheme and cumulus parameterization. A summary of the models' cloud and convective schemes (Table 2) are briefly explained. Model physics are identical for the coarse and fine resolution simulations.

[10] Convective parameterizations in these models are all based on the mass flux framework using either a single updraft/downdraft plume couple (IFS, HIRAM, MetUM, and GME) or multiple updraft plumes (CAM4, GAMIL, AM2, AM3, and JMA). The coupling with the large-scale model is done, however, by passing only a single average (bulk) convective tendency. Key aspects of climate models are highly sensitive to entrainment specification in the convective parameterizations [e.g., *Gregory et al.*, 1997; *Bechtold et al.*, 2008]. A nice summary with analytical expressions of entrainment and detrainment was recently given by *de Rooy and Siebesma* [2010]. For multiplume models, entrainment can be a complicated function of the environment though a simple treatment is applied to a single plume [e.g., *Moorthi and Suarez*, 1992]. For a bulk plume parametrization, entrainment is more straightforward and easy to control [*Plant*, 2010]. Entrainment rate is generally specified as an inverse to the plume depth (AM2, HIRAM) or radius (GME, AM3) and has no variation with height, but some models use height varying entrainment (MetUM, IFS). Most models include only the turbulent entrainment, but IFS includes both turbulent entrainment and dynamic entrainment sensitive to relative humidity [*Bechtold et al.*, 2008]. CAM4 uses a dilute plume sensitive to the free troposphere humidity [*Neale et al.*, 2008]. Other detailed implementation, such as the mass flux closure, CAPE computation, and CAPE adjustment or consumption time scales, differ among the models. This will impact the convective heating structure and precipitation partitioning.

[11] Cloud macrophysics in these models can be divided into two groups, one is prognosed (AM2, AM3, IFS) following *Tiedtke* [1993], and the other is diagnosed from relative humidity (CAM4, IAP, and GME) or total water PDF considering subgrid scale variability (MetUM, HIRAM, JMA). Cloud microphysics, including the treatment of precipitation and hydrometeor sedimentation, are more diverse among these models. For example, some models consider the particle size distribution, while others simply parameterize various microphysical processes as a function of ice or liquid water mixing ratio directly. This is expected to impact model cloud properties (e.g., ice and liquid water content and their vertical distribution) significantly. Note that standard AM3 predicts cloud droplet number including aerosol activation [*Donner et al.*, 2011], but the simulation in this study uses the same prescribed cloud droplet number as AM2 and HIRAM.

3. Results

[12] Comparing observations collected during the TWP-ICE field experiment with model output at varying model grids is nontrivial. First, there are spatial and temporal inconsistency between observations and model. For example, retrievals of liquid and ice contents are generally point measurements with high temporal resolution, while model cloud quantity generally represents an in-cloud or grid-box mean. Second, some model variables may not represent exactly the same quantity as observations or observational retrievals. For example, IWC in some models includes snow, while others not. Finally, the observations used in this study are mostly the area mean (i.e., within the variational analysis polygon in Figure 1). We use the average of the model grid points residing in a box covering the polygon (Figure 1) for most comparisons unless explicitly noted. Model grid points overlapping with the box vary from 2 for the coarsest model to over one hundred grid points for models at ~20 km resolution. The total area sampled in the models varies from ~90,000 to 150,000 km^2 while the observational area is ~70,000 km^2; these differences are small compared to the variations between the models. Before investigating the model performance during different regimes, we first present the time variation of some key variables for the whole period. The comparison focuses on the period from 19 January to 12 February, 2006.

3.1. Model General Behavior

[13] Figure 2 shows the evolution of winds and moisture at 700 hPa from the ECMWF analyses and outgoing longwave radiation (OLR) and surface precipitation from the satellites with one example model forecast. The TWP-ICE period is coincident with the activity of a major MJO event. The wet period (19–25 Jan) was an active monsoon period dominated by robust oceanic convection with a mesoscale convective system (MCS) developing into a tropical low informally dubbed "Landphoon John" that moved south inland near

Table 1. Participating Models[a]

Model	Model Full Name	Modeling Center	References
IFS	Integrated Forecasting System	ECMWF	ECMWF (IFS documentation, 2008, http://www.ecmwf.int/research/ifsdocs 2008)
CAM4	Community Atmospheric Model version 4	NCAR	*Gent et al.* [2011]
AM2	Atmospheric Model version 2	GFDL	*GFDL Global Atmospheric Model Development Team* [2004]
AM3	Atmospheric Model version 3	GFDL	*Donner et al.* [2011]
HIRAM	High-resolution AM2	GFDL	*Zhao et al.* [2009]
MetUM	Met Office Unified Model	UK Met Office	*Martin et al.* [2006]
JMA	Global Spectral Model	JMA	*Japan Meteorological Agency* [2007]
GME	GME Global model	DWD	*Majewski et al.* [2002]
GAMIL	Grid point Atmospheric Model of IAP LASG	IAP LASG	LASG (http://www.lasg.ac.cn/FGCM/ArticleShow2.asp?BigClass=Mode%20Documentation&ArticleID=4229)

[a]Acronyms in the table are: ECMWF (European Centre for Medium-range Weather Forecasts); NCAR (National Center for Atmospheric Research); GFDL (Geophysical Fluid Dynamics Laboratory); JMA (Japan Meteorological Agency); DWD (German Weather Service); IAP (Institute of Atmospheric Physics); LASG (Laboratory of Numerical Modeling for Atmospheric Sciences and Geophysical Fluid Dynamics).

30 Jan at 20°S (Figure 2a). As this tropical low moved south, middle troposphere dry air intruded from the midlatitudes, and deep convection was suppressed over Darwin near 12°S, with cumulus congestus dominating during this dry period (26 Jan–2 Feb). The third period is a short three-day clear period without precipitation near Darwin. The fourth period is a monsoon break period with more localized afternoon thunderstorms accompanying the land-sea breeze and several squall lines crossing Darwin (6–13 Feb) accompanied by a strong high pressure system residing inland to the south. Corresponding to these regimes, OLR and precipitation show concomitant variation with a clear rain shaft following the southward drift of the tropical low (Figure 2b). There were thunderstorms in the afternoon and early evening near the coast area during the break period (Figure 2b). Further inland, a strong diurnal cycle of land surface temperature is obvious in the OLR fields during the break period.

[14] The time-latitude plots from the 25-km CAM4 (Figures 2c and 2d) indicate that the CAPT approach effectively gives realistic large-scale environments and captures the transition of these regimes well. For example, the strong westerlies followed by the passage of an active MJO phase and the south moving tropical low are well captured. The model also captures the mid-troposphere dry air intrusion near Darwin around 3 Feb. In the break period, large-scale forcing is relatively weak. The model captures the land sea temperature difference and triggers localized convection, though the magnitude is relatively weak and timing is not exactly the same. Other models also capture the overall large-scale environment well (not shown).

[15] Figure 3 shows the daily mean observed and model surface downward shortwave (SWDSFC), OLR, ice water path (IWP), liquid water path (LWP), water vapor path (WVP), and total precipitation rate (PR), respectively. Overall, the models capture the inter-regime characteristics well, like the less SWDSFC and OLR in the wet regime than the dry and break regime. All models tend to underestimate WVP in the wet and break period. Most models predict the maximum precipitation near 25 Jan, which is one day later than the observed. This maximum precipitation shift was also noted in *Boyle and Klein* [2010] and was attributed to the operational analysis used. The maximum vertical motion in the ECMWF operational analysis near Darwin region is around one day later than the variational analysis (not shown). Observed OLR increases from ~150 W m^{-2} in the wet period to ~250 W m^{-2} in the clear period and decreases slightly during the break period. Most models tend to overpredict OLR except HIRAM and AM3, which tend to underpredict OLR, especially during the dry and break periods. Model SWDSFC is generally within 50 W m^{-2} of the observed and also shows a one day shift of the minimum consistent with the precipitation shift. The two observational LWP retrievals, especially the one including drizzle and rain, show a corresponding variation with PR. For example, LWP is up to 0.4 mm near 23 Jan with a PR of 75 mm day^{-1}. LWP differs by up to two orders of magnitude among the

Table 2. Characteristics of Participating Models and Investigators[a]

Name	Convection	Large-Scale Cloud	Resolution (km)	Investigator
IFS (ECMWF)	Tiedtke89/Bechtold	Tiedtke/Tompkins	125/25/91 L	P. Bechtold
CAM4 (NCAR)	ZM95/Hack	RK/Zhang	200/25/26 L	J. Boyle
AM2 (GFDL)	RAS	Tiedtke/Rotstayn	250/24 L	Y. Lin
AM3 (GFDL)	Donner/UW	Tiedtke/Rotstayn/Ming	250/48 L	Y. Lin
HIRAM (GFDL)	UW	Tiedtke/Rotstayn/Zhao	250/50/32 L	M. Zhao
MetUM (Met Office)	GR-Martin	Smith90/Wilson-Ballard	50/70 L	M. Willett
GSM (JMA)	RAS/Pan-Randall	Smith90/Sundqvist	60/20/60 L	T. Komori
GME (DWD)	Tiedtke89	RH83	40/40 L	K.Wapler, A. Seifert
GAMIL (IAP)	ZM95/Hack	MG08	280/100/26 L	X. Xie, L. Dong

[a]Acronyms in the table are: Tiedtke89 [*Tiedtke*, 1989]; Bechtold [*Bechtold et al.*, 2008]; Tiedtke [*Tiedtke*, 1993]; Tompkins [*Tompkins*, 2002]; ZM95 [*Zhang and McFarlane*, 1995]; Hack [*Hack*, 1994]; RK [*Rasch and Kristjansson*, 1998]; Zhang [*Zhang et al.*, 2003]; RAS (Relaxed Arakawa and Schubert) [*Moorthi and Suarez*, 1992]; Rotstayn [*Rotstayn*, 1997]; Ming [*Ming et al.*, 2006]; Zhao [*Zhao et al.*, 2009]; Donner [*Donner*, 1993; *Donner et al.*, 2001]; UW (University of Washington) [*Bretherton et al.*, 2004]; GR [*Gregory and Rowntree*, 1990]; Martin [*Martin et al.*, 2006]; Smith90 [*Smith*, 1990]; Wilson-Ballard [*Wilson and Ballard*, 1999]; Pan-Randall [*Pan and Randall*, 1998]; Sundqvist [*Sundqvist et al.*, 1989]; RH83 [*Rutledge and Hobbs*,1983]; MG08 [*Morrison and Gettelman*, 2008]. Model vertical levels are also denoted in the resolution column.

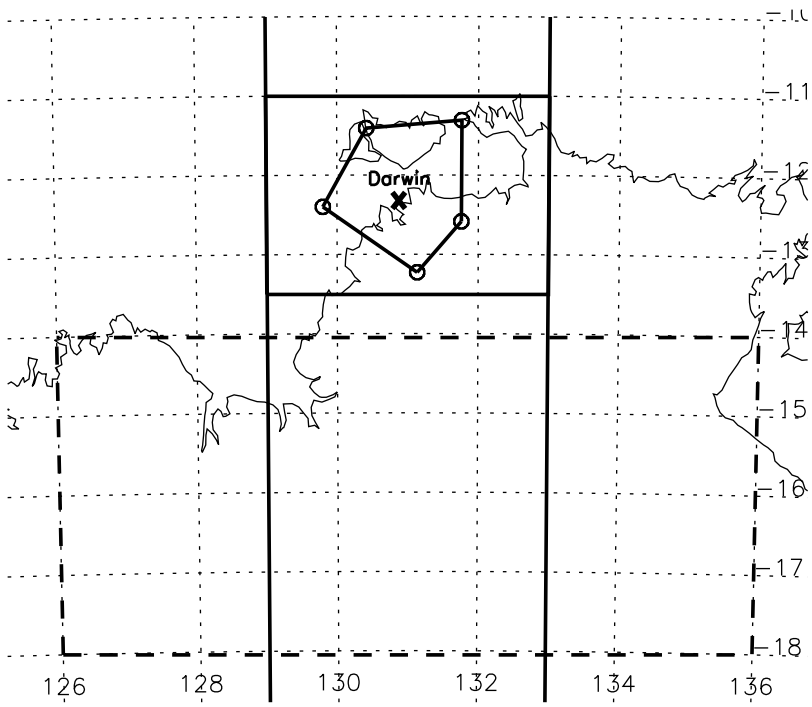

Figure 1. TWP-ICE field experiment domain with sounding sites (circles) and Darwin (cross) denoted. The solid line box is the region where model forecasts are averaged. The dashed line box denotes the region used for the precipitation diurnal cycle as shown in Figure 8. The two solid lines denote the longitudes in which the mean is computed for the time-latitude plot in Figure 2.

models, with GAMIL and MetUM having LWP up to 1.5 and 0.9 mm, respectively. Observational retrievals of IWP are large (0.1 to 0.15 mm) during the wet and break period with small IWP during the dry period. Though most models capture this inter-regime variation of IWP, IWP also differs by up to two orders of magnitude among the models. Three GFDL models, IFS and MetUM have large IWP in the wet period. Overall, this is consistent with *Waliser et al.* [2009], who found large variation of IWP and LWP among the models they compared. One source for the substantial discrepancies of cloud simulations is from the cloud scheme, which is designed and implemented differently among the models.

[16] Cloud amounts also differ significantly among the models (Figure 4). Note that model cloud fraction represents the fraction of a model grid box occupied by clouds, while observational cloud fraction is derived from the cloud occurrence frequency at a single point [cf. *Xie et al.*, 2008]. For this reason, the comparison here can be only taken qualitatively. Note the model cloud fraction uses the closest grid point value. There are again four distinct regimes in the observed clouds, a wet period with extensive clouds extending from the surface to the upper troposphere, the suppressed and dry period with congestus and an upper level cirrus deck advected from the tropical low in the south, and the break period with more intermittent deep convection with a small coverage of upper level cirrus. We found that resolution only has minor impacts on cloud fields (not shown) and this implies that the model physics (most probably the cloud and convection schemes) dominates model cloud fields. Models generally get the transition from strongly forced to weakly forced large-scale conditions, but only some get the transition from the dry to break conditions. For example, GAMIL, MetUM, and GME cannot depict the congestus associated with the dry air intrusion during the dry period. Compared with AM2, AM3 has more clouds in the upper troposphere (~50 hPa). JMA, CAM4, and IFS capture the shallow convection (congestus) relatively well during the dry period compared with other models. In the break period, models capture the deep convection well, though some models cannot distinguish cloud fields between the break and dry period. Other fields, such as water vapor, temperature, and winds are also compared (not shown), and there are generally no significant differences among the models. This is further evidence that the cloud and convection schemes are the primary difference makers between simulations.

3.2. Regime Specific Evaluation

[17] The distinct cloud and precipitation characteristics associated with the three regimes (wet, dry, and break as shown in Figures 3 and 4) provide a good test of the model cloud and convection performances under different environmental conditions. In this section, model simulations in each regime are compared, using available observations as references. Figure 5 shows the profiles of LWC, IWC, cloud fraction (CF), and relative humidity (RH) with respect to water for the three periods, respectively. Since cloud microphysical retrievals are available only in cloud, model in-cloud (grid box mean value divided by cloud fraction) LWC and IWC are compared for consistence. As mentioned before, two LWC retrievals are shown here. One considers drizzle and rain besides cloud droplet, while the other only includes cloud droplet. LWC retrieval is around 0.1–0.3 g kg^{-1} and decreases quickly to zero above 400 hPa for all the three periods. Though

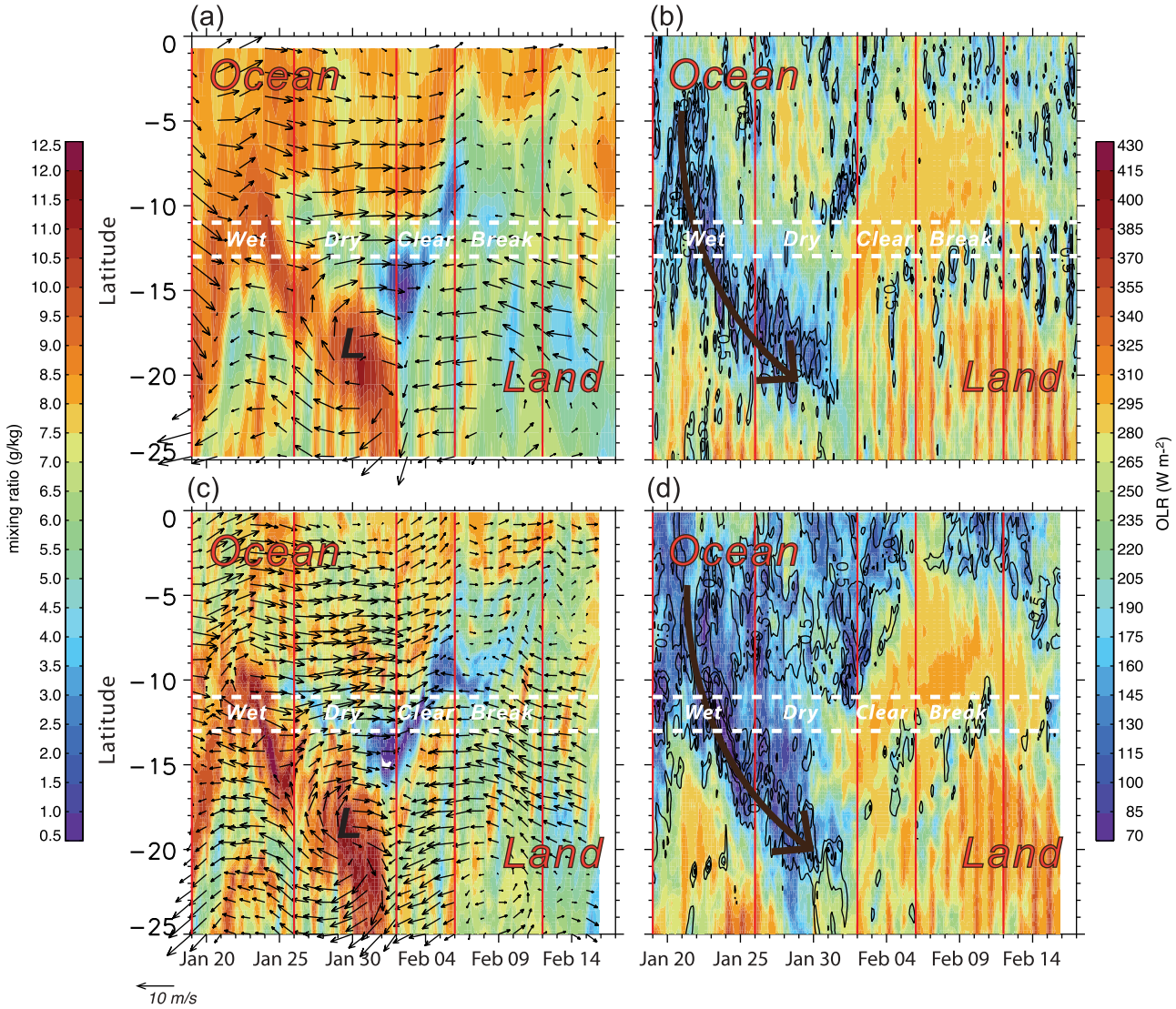

Figure 2. (a) Time-latitude plot of wind vectors and specific humidity (g/kg, shaded) at 700 hPa from the ECMWF operational analysis. (b) Time-latitude plot of OLR (shaded) from the European Union CLoud Archive User Service (CLAUS) with precipitation (mm/h) from TRMM 3B42 overlaid (contours) during the same period. (c) Same as Figure 2a but from the 25-km CAM4 day 2 forecasts. (d) Same as Figure 2c but showing the OLR and precipitation field. The four periods in the TWP-ICE region are also labeled. All data used is every 3 h.

models have similar LWC profiles among the three periods, LWC inter-model differences are large for each period. GAMIL predicts maximum LWC near 600 hPa in the wet and dry period, and CAM4 tends to have large LWC near the surface. MetUM predicts relatively large LWC (up to 0.8 g kg^{-1}) and GME has negligible LWC. Different from observational retrievals, CAM4, MetUM, and GAMIL have substantial LWC above 400 hPa.

[18] During the wet period, IWC retrievals reach ~0.1 g kg^{-1} near 300 hPa with the mean and standard deviation up to 0.5 g kg^{-1} near 100 hPa. One retrieval, specifically designed for cirrus [*Deng and Mace*, 2008], derived large IWC at these upper levels. We include this retrieval considering that there are extensive anvils and upper level cirrus during the wet period, which may be significantly underestimated by MMCR due to signal attenuation as discussed later. In the dry period, there are IWC up to 0.07 g kg^{-1} near 200 and 400 hPa corresponding to the upper level cirrus deck and some cumulus congestus reaching the middle troposphere (cf. Figure 4a), respectively. IWC retrievals in the break period are up to 0.3 g kg^{-1} with larger standard deviation than those in the wet and dry period. The larger IWC in the break period than in the wet period seems surprising at first sight. We note the continental type convection during the break period sometimes has more intense measured reflectivity than that in the wet period. These high reflectivity values are likely associated with hail and it is possible that the IWC in these very high reflectivity regions is overestimated by the retrievals. *May and Ballinger* [2007] also note the convection in the break period tends to be more intense with higher reflectivity and higher cell heights. Similar to IWP comparison, IWC among the models differs

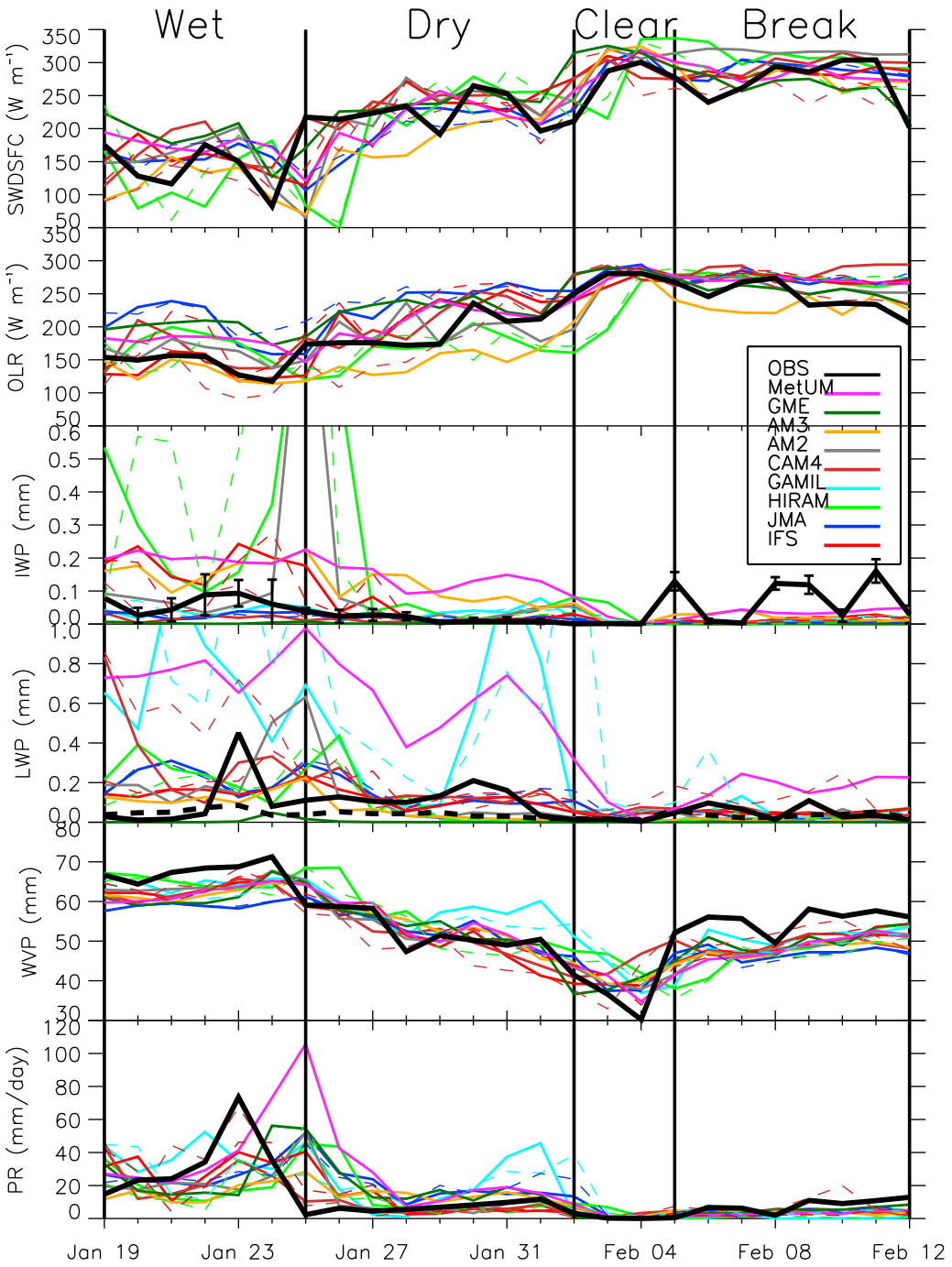

Figure 3. Time series of daily mean surface downward shortwave (SWDSFC), outgoing longwave radiation (OLR), ice water path (IWP), liquid water path (LWP), water vapor path (WVP), and total precipitation rate (PR) from models and observational estimates. Error bar in the IWP panel is the standard deviation of 5 IWP retrievals from CRED. The thick solid and dashed black lines in LWP panel are the two observational retrievals from CRED. The four distinct periods are also labeled. Dashed lines are fine resolution model results.

significantly with HIRAM having the largest IWC. MetUM, IFS, and GFDL models generally have larger IWC than other models, with GME having the smallest IWC. Much smaller LWC and IWC in GME is because convective cloud contribution is excluded. IWC extends below the melting level for MetUM, suggesting that the ice and snowmelting treatment in this model might be different from the instantaneous melting used in other models. Overall, similar to LWP and IWP, LWC and IWC differs by up to two orders of magnitude among the models, consistent with previous studies [*Waliser et al.*, 2009]. Nevertheless, observational retrievals with an uncertainty estimate still provide a useful constraint and guidance for model development.

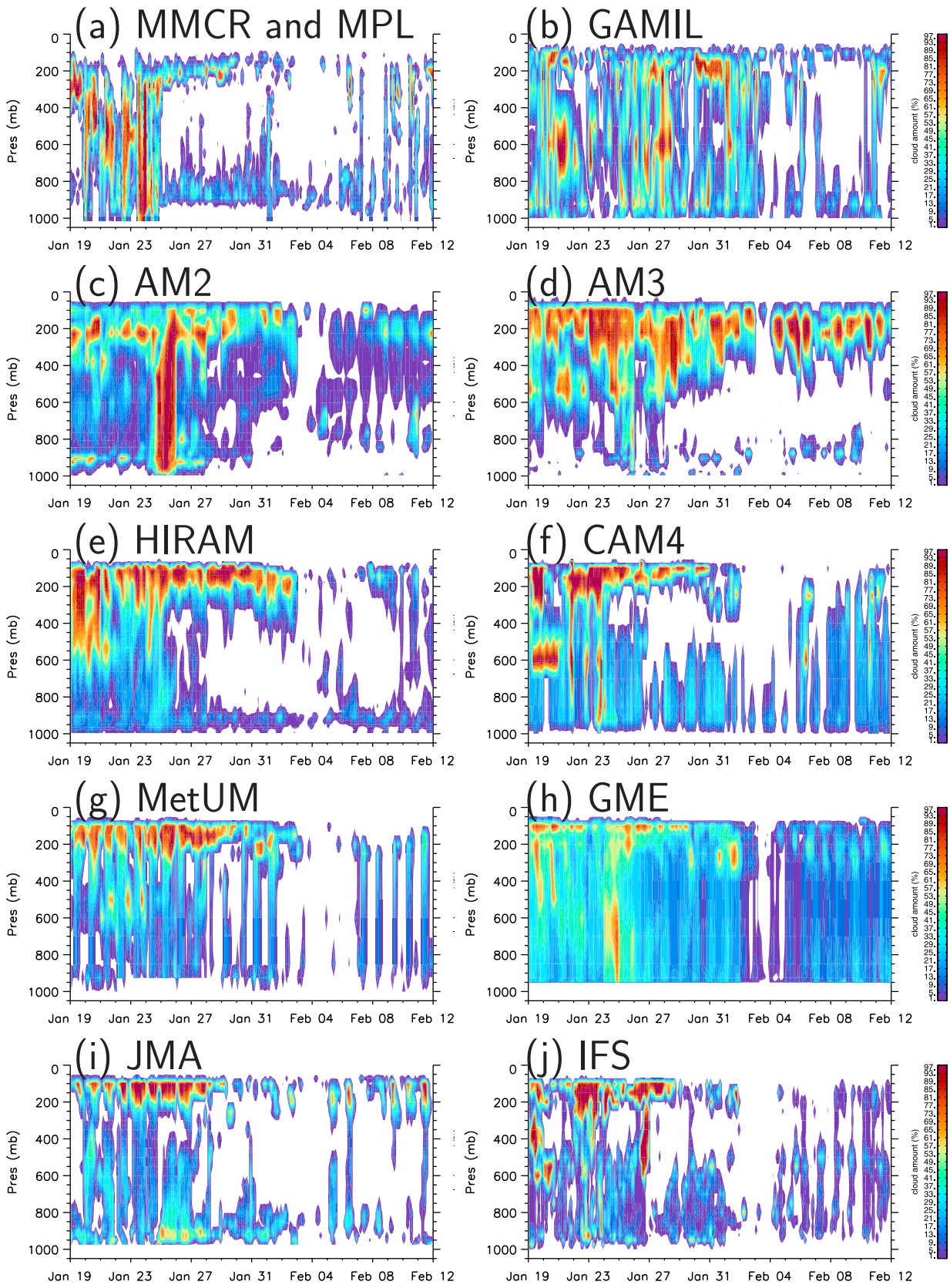

Figure 4. Time-pressure plot of cloud fraction from (a) MMCR and MPL, (b) GAMIL, (c) AM2, (d) AM3, (e) HIRAM, (f) CAM4, (g) MetUM, (h) GME, (i) JMA, and (j) IFS. Model results are fine resolution forecasts when available.

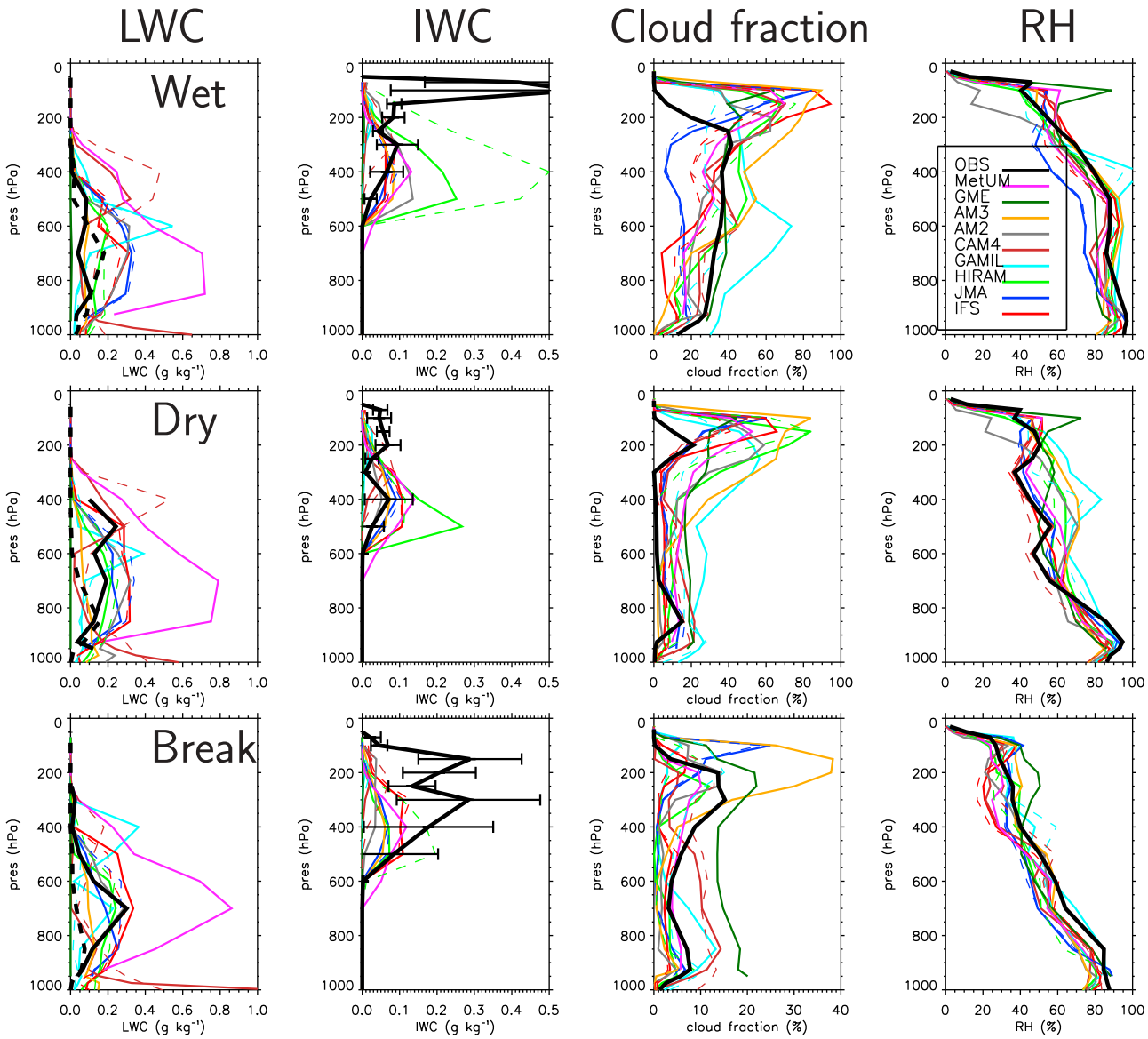

Figure 5. Mean profiles of (first column) in-cloud LWC, (second column) IWC, (third column) cloud fraction, and (fourth column) relative humidity with respect to water for the (top) wet, (middle) dry, and (bottom) break period from models and available observational estimates. The thick solid and dashed black lines in the first column are the two observational retrievals from CRED. Error bar in the second column is the standard deviation of 5 IWC retrievals from CRED. Dashed lines are fine resolution model results. Note the different *x* axis scale for cloud fraction.

[19] In the wet period, most models have top-heavy cloud fraction approaching 40–90% near 150 hPa, while observed CF decreases significantly above 250 hPa. This is probably due to the significant signal attenuation of the MMCR in the presence of deep convective clouds. Satellite images indicate extensive upper level clouds over Darwin region in the wet period and suggest the abrupt CF drop-off above 250 hPa is somewhat unrealistic. JMA has a minimum of CF near 400 hPa, coincident with the model's dryness in the middle-upper troposphere compared with other models and observations. Model RH is generally within 10% of the observed except at the middle and upper-troposphere for JMA and above 200 hPa for AM2 and GME. GAMIL is saturated near 400 hPa due to a ~3 K cold bias there (Figure 6). There is an obvious observed dipole of cloud fraction corresponding to shallow congestus and the upper level cirrus deck in the dry period. Models tend to overpredict the middle and upper layer clouds by 2–4 times during this period. This suggests that models have difficulty simulating congestus, with convective plumes shooting into the dry layer too frequently. Observed RH decreases quickly from 90% in the boundary layer to ~60% above 700 hPa in the dry period as a result of the dry air intrusion. RH spread among the models is larger during the dry period, especially in the middle troposphere with an overall moist bias for most models. During the break period, the MMCR and MPL measured the smallest CF with maximum CF of 15% near 300 hPa. Models have lower CF in this period, although AM3 predicts CF up to 40% near

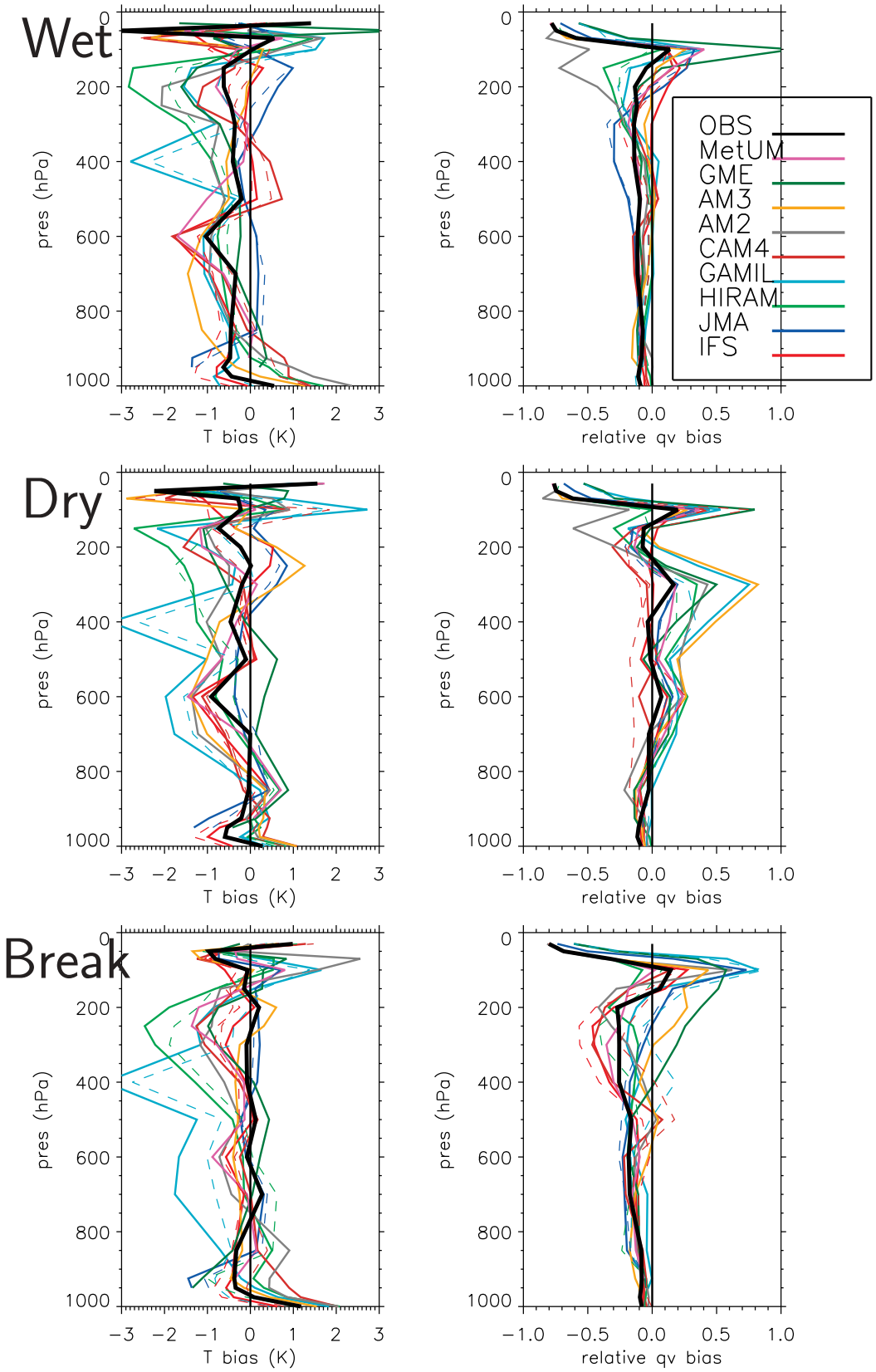

Figure 6. Mean profiles of (left) temperature bias and (right) water vapor mixing ratio relative bias with respect to the variational analysis for the (top) wet, (middle) dry, and (bottom) break period. The black thick lines denote the bias of the ECMWF analysis relative to the variational analysis. Dashed lines are fine resolution model results.

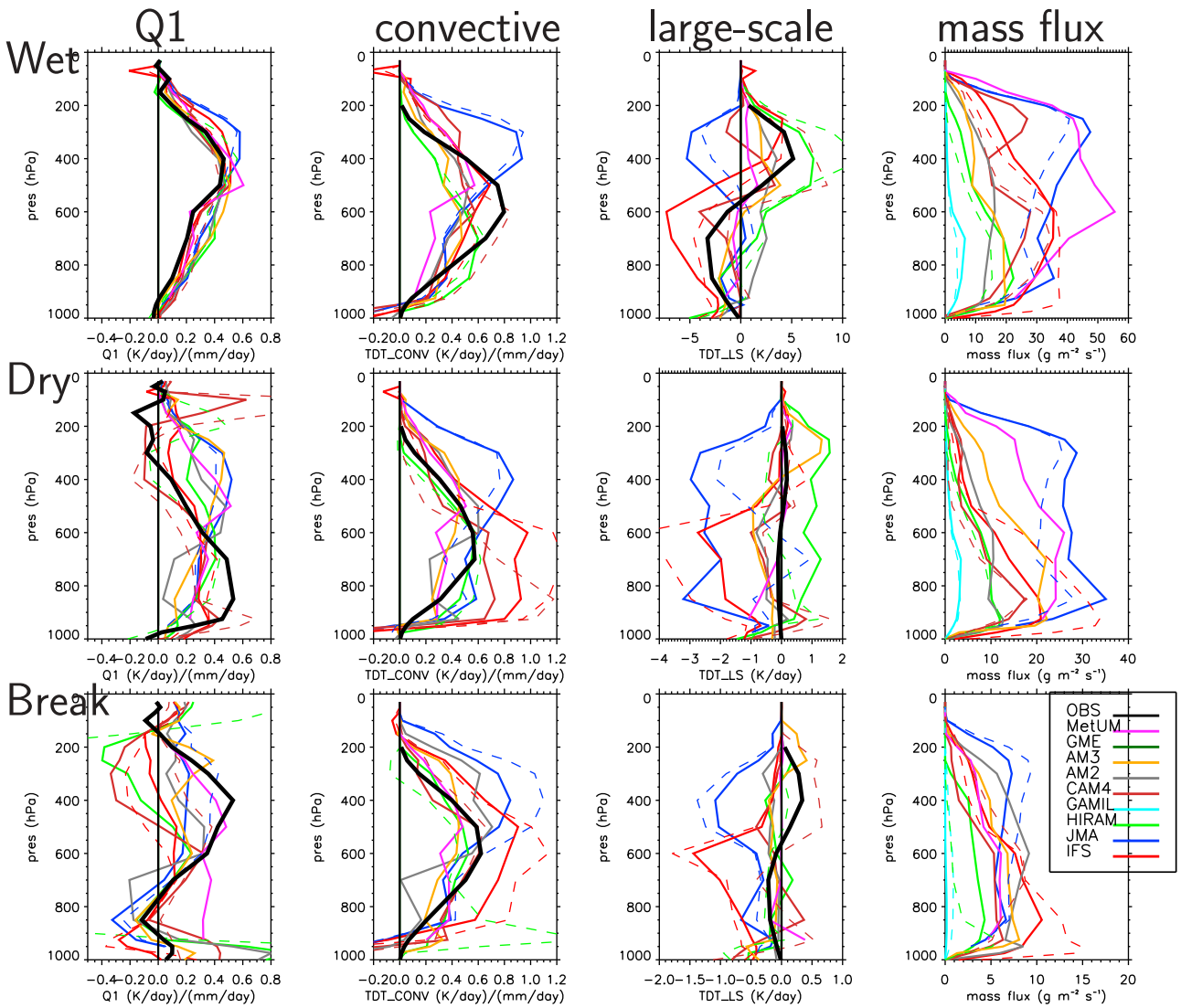

Figure 7. Mean profiles of (first column) total precipitation normalized Q1, (second column) convective precipitation normalized convective heating, (third column) stratiform heating, and (fourth column) convective mass flux for the (top) wet, (middle) dry, and (bottom) break period from models and available observational estimates. Dashed lines are fine resolution model results. Note the different *x* axis scale for the third and fourth columns.

200 hPa. RH in the break period varies with heights as observation, but most models show a dry bias, which is opposite to the dry period.

[20] RH comparison in Figure 5 indicates the models have different temperature and moisture profiles. Model systematic temperature and moisture biases can be detected by the CAPT approach [*Willett et al.*, 2008; *Martin et al.*, 2010]. Figure 6 shows the temperature and moisture bias of model forecasts relative to the variational analysis over the three periods. Note that RH bias is impacted by both temperature and moisture bias following the Clausius-Clapeyron equation. Some overall features in Figure 6 are summarized here. First, the ECMWF analysis, from which the models are initialized, is drier by 10–20% compared to the variational analysis during the wet and break period. As reasons for this discrepancy, one can cite a different handling of observation errors for the microwave retrievals, different radiosonde bias corrections, different model background, and the fact that the ECMWF analysis also includes information from the larger scales. This dryness in the initial condition may contribute to the dryness in model forecasts. Second, all models unanimously underestimate moisture below 600 hPa in the wet and break period. In contrast, most models (except IFS and CAM4) tend to have a moist bias (up to 80% near 300 hPa for GAMIL and AM3) above ~700 hPa in the dry period. This is consistent with Figure 4, which shows IFS and CAM4 have good simulation of shallow congestus, but GAMIL and AM3 forecast too much clouds around 300 hPa. IFS and CAM4 use an entrainment rate dependent on the free troposphere humidity [*Bechtold et al.*, 2008; *Neale et al.*, 2008] and increase the sensitivity of convection development to the environmental humidity. As the convection depth is overestimated, moisture is transported upward to a higher layer (not shown) than the observed and results in the

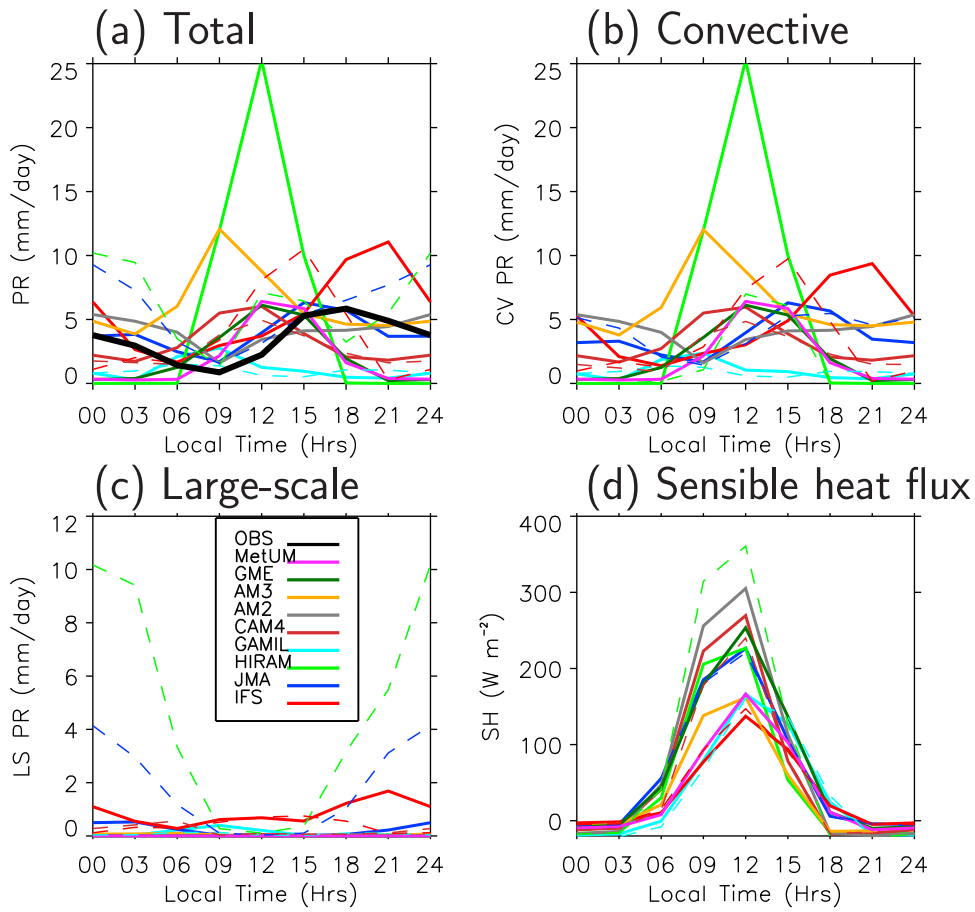

Figure 8. (a) Diurnal cycle of total precipitation rate averaged over the dashed box in Figure 1 during the break period (Feb 6–13). Black line denotes the precipitation rate from TRMM 3B42 retrievals. (b) Same as Figure 8a but showing the convective precipitation rate. (c) Same as Figure 8a but showing the large-scale precipitation rate. (d) Same as Figure 8a but showing the sensible heat flux. Dashed lines are fine resolution model results.

moist bias in most models. It appears that the moist bias in the dry period is related to the poor forecasts of cumulus congestus in some models. Temperature bias is more diverse among the models and generally less than 2 K in the troposphere except for HIRAM and GAMIL. HIRAM tends to be cold in the upper troposphere near 200 hPa. GAMIL has a maximum cold bias up to 3 K near 400 hPa. Such temperature and moisture bias are related with the vertical heating and moistening structures discussed later.

[21] Vertical heating structures are different for convective and stratiform precipitation. They are a good test of model convective parameterizations in terms of their cloud model, i.e., how to distribute the heating and moistening in the vertical [*Bechtold et al.*, 2001]. Following *Lin et al.* [2004], Figure 7 shows the precipitation-normalized Q_1 (Q_1 divided by total precipitation), precipitation-normalized convective heating (convective heating divided by convective precipitation) and stratiform heating (not normalized because some models have very small large-scale precipitation), and cumulus mass flux during the three periods. Q_1 is from the variational analysis [*Xie et al.*, 2010] and convective and stratiform heating are from Courtney Schumacher (personal communication, 2012). These retrievals are subject to an uncertainty of at least 25% associated with the surface precipitation retrieval from the C-POL radar [*Fridlind et al.*, 2012]. During the wet period, all models capture the top heavy Q_1 profile quite well and the differences among the models are small. This is due to the fact that the large-scale forcing in the active monsoon environment is strong and the response to such a strong forcing is well captured by these models. Most of the Q_1 is from the convective component, which has a maximum near 600 hPa. All other models maximize between 500 and 700 hPa except JMA, which has the convective heating maximizing near 400 hPa. HIRAM tends to have bottom-heavy convective heating. Observationally retrieved stratiform heating is up to 5 K day^{-1} and has a distinct structure featuring heating aloft and cooling below. Stratiform heating is more diverse among the models. Similar to observations, IFS, MetUM, AM3, and HIRAM have condensational and depositional heating above and evaporative and melting cooling below. JMA has stratiform cooling aloft near 400 hPa, which effectively compensates for the overestimated convective heating at that height. Convective mass flux profiles are generally similar to convective heating profiles with the heating maximum slightly above the mass flux maximum. However, the magnitude of the convective mass flux differs significantly among the models, with GAMIL having the smallest value (~5 g m^{-2} s^{-1}) and MetUM and

JMA having larger values (~50 g m^{-2} s^{-1}). MetUM and CAM4 have a mass flux maximum near the freezing level and JMA has a shallow mode for the mass flux.

[22] In the dry period, deep convection is inhibited and congestus extends to 600 hPa (Figure 4). Observed Q_1 indicates a bottom heavy heating structure associated with the shallow convection. Model Q_1 profiles are more varied than those in the wet period with IFS, CAM4, and 50-km HIRAM capture the bottom heavy profile relatively well. These models also have small moisture bias above 700 hPa as shown in Figure 6. In contrast, models having deep convective heating and deep convective mass flux also have convective moistening above 700 hPa (not shown), which contributes to the moist bias in these models. This is a good example illustrating the close connection between convective parameterization and model's systematic bias. Compared with the observed Q1, observed convective heating peaks at a higher level (700 hPa). Most models somewhat capture the observed convective heating profile, but JMA still has the convective heating at too high an altitude. Consistent with *Derbyshire et al.* [2004], models using entrainment rate specification considering the moisture effect (IFS and CAM4) are able to capture the bottom heavy heating profile due to the sensitivity to the middle level humidity. Again, stratiform heating differs significantly among these models. Furthermore, most models overestimate the negligible stratiform heating observed and fail to capture the characteristic stratiform heating profile shape. Convective mass flux possesses a bottom-heavy profile associated with the inhibited convective depth for most models except JMA, which has a deep mode besides a well-defined shallow mode. Consistent with the convective heating profile, CAM4 and IFS have the most bottom-heavy profile of mass flux.

[23] In the break period, Darwin area is dominated by intense afternoon convection and squall lines forming on sea breeze convergence lines as well as moving off the higher terrain inland (Figure 4). The continental type convection is more intense and generally relatively small spatially than the oceanic convection during the wet period. These convective systems tend to have much smaller stratiform precipitation as indicated by the negligible stratiform heating (Figure 7). Models respond somewhat correctly and simulate the observed total heating structures, which has cooling in the boundary layer and a broad heating in the 300–600 hPa layer. This boundary layer cooling is probably due to rain evaporation in the relatively dry near surface air. 50-km HIRAM has total precipitation rate less than 1 mm day^{-1} in the break period and Q1 is dominated by the longwave cooling in the troposphere (not shown). This is the reason why its normalized Q1 profile is negative and out of the bound in Figure 7. Similar to the dry period, convective heating is more diverse among the models. This suggests the response of the models to the relatively weak forcing during the dry and break period are more diverse. Stratiform heating becomes small (<1 K day^{-1}) with structures being varied among the models. Compared to the dry period, the break period magnitudes of convective mass flux are decreased by one-half and this is probably due to the less frequent convection occurrence in the break period. Overall, most models somewhat capture the shapes of convective heating associated with different types of convection, especially in the wet period. In contrast, stratiform heating shape is more diverse among the models and many models cannot capture the characteristic profile with heating aloft and cooling at low levels. This not only highlights the importance of the cloud and microphysics representation but also the coupling of the convection to the cloud scheme.

[24] In all the three periods (Figure 7), we note that GAMIL has the smallest convective mass flux with a bottom-heavy profile (approaching zero above 400 hPa). HIRAM also has relatively small convective mass flux and a bottom-heavy convective heating profile (approaching zero above 200 hPa). Such small convective heating in the upper troposphere is closely related to the upper level cold bias in these two models (Figure 6). It is worth noting that the upper level cold bias in climate simulations is generally not as large as that in these short-term forecasts [*Zhao et al.*, 2009].

3.3. Resolution Impact

[25] With increased computer power, AGCMs are running at higher resolutions. Some global operational forecast models are regularly run at a resolution of ~20 km (Table 2). For climate models, there are also active studies to understand the resolution benefit [*Boyle and Klein*, 2010, and references therein]. These studies suggest that the topography is better resolved at higher resolution and local-scale circulations are better described. However, the overall improvement is moderate and some inherent biases are not ameliorated by resolution only. One relatively robust result from these studies is the increase of large-scale (L-S) precipitation at higher resolution [*Lau and Ploshay*, 2009; *Boyle and Klein*, 2010]. This is also the case here with the fine resolution forecasts generally having more L-S precipitation than the coarse resolution forecasts (not shown).

[26] Considering that identical physics are used in different resolution simulations, we expect to see similar cloud properties between high and low resolution simulations. This is generally the case, especially for the IWC and LWC vertical structures (Figure 5). For example, LWC peaks near 600 hPa for the two IAP simulations. Two JMA models produce very close LWC, IWC, and CF profiles. In terms of temperature and moisture bias, high resolution does not necessarily reduce those biases (Figure 6), which is mostly characterized by model's physical parameterizations. We see the vertical structures of various heating terms and convective mass fluxes are also similar between the high and low resolution simulations (Figure 7). Stratiform heating generally increases with resolution, especially during the wet period (Figure 7). Fine resolution is more favorable for shallow convection, at least for IFS in terms of the mass flux (Figure 7). At higher resolution, more lower boundary inhomogeneity, such as terrain and soil moisture, are introduced. This increases the inhomogeneity of near surface thermodynamic fields and thus the probability of convection occurrence and intensity variations.

[27] The diurnal cycle of precipitation has long been a challenge to numerical models [*Betts and Jakob*, 2002; *Dai and Trenberth*, 2004; *Yang and Slingo*, 2001; *Bechtold et al.*, 2004; *Dirmeyer et al.*, 2012]. To analyze the resolution impact on the precipitation diurnal cycle, we focus on a

box (the dashed box in Figure 1) over the coastal and inland region near Darwin, where satellite observations show a relatively robust diurnal cycle during the break period (Figure 2b). TRMM retrievals reveal a late afternoon/early evening precipitation maximum (Figure 8). Most models possess a robust precipitation diurnal cycle dominated by convective precipitation peaking from near noon (low resolution HIRAM, MetUM, CAM4, and GME) to late afternoon (JMA and IFS). Such robust diurnal cycle of convection over land is closely related to the strong diurnal cycle of surface sensible (Figure 8d) and latent heat flux (not shown) though its phase may lag behind the heat flux phase. The diurnal cycle in AM2 is modulated by the relatively long relaxation time ($\sim$12 h) used in RAS. Total precipitation is generally dominated by convective precipitation except for the high-resolution JMA and HIRAM, which have substantial (4 and 10 mm day^{-1}) L-S precipitation near midnight (Figure 8c). As a result, the total precipitation diurnal cycle is significantly modified. Convective precipitation is able to extend to nighttime in most models. Overall, the impact of resolution on the precipitation diurnal cycle is relatively small unless the resolution significantly modulates the precipitation partitioning (e.g., HIRAM and JMA). 125-km IFS has both L-S and convective precipitation peaking in the evening, while 25-km IFS precipitation is mainly convective with a peak in the afternoon. The resolution dependence in the phase of the diurnal cycle can be attributed to the horizontally variable and resolution dependent CAPE adjustment time scale [*Bechtold et al.*, 2008], which in the IFS is of O(20–60 min) for the 25-km resolution and of O(1–3 h) for the 125-km resolution. A longer adjustment time scale favors a smoother evolution and a shift of the precipitation peak from noon to the afternoon and early evening. Overall, the model precipitation diurnal cycle over the tropical land area is dominated by the convective parameterization when L-S precipitation is negligible. As resolution increases, L-S precipitation might increase and modify the total precipitation diurnal cycle. Due to the short time period and the small area considered in this study, these results need to be further evaluated and confirmed in the future.

4. Summary

[28] An intercomparison of global atmospheric model simulations of tropical convection has been presented and evaluated with available observations collected during the TWP-ICE field experiment. Short simulations initialized from the ECMWF analysis have been used to constrain model large-scale states and thus isolate model systematic biases originating from various physical parameterizations. With realistic thermodynamic and kinematic fields captured in various weather regimes (wet, dry, and break), model precipitation, cloud properties (LWC, IWC, cloud fraction), radiation, and vertical heating profiles respond accordingly in these regimes. Despite somewhat realistically simulated precipitation, there are substantial cloud property discrepancies among the models, which are mainly influenced by cloud and convective parameterizations. For example, IWC and LWC differ by up to two orders of magnitude among these models. Nevertheless, observational retrievals with the uncertainty estimate provide constraint and guidance for model development regarding cloud simulations.

[29] Compared with the relatively consistent response of total and convective heating to the strong forcing in the wet period, the model responses in the dry and break period are more diverse when the forcing is relatively weak. Cumulus congestus in the dry period are poorly simulated by most models and the overestimated deep convection results in a moist bias above the congestus top (700 hPa) in these models. Compared with the bottom-heavy heating profile observed in the dry period, these models tend to have heating reaching an altitude too high. Models (CAM4 and IFS) with their convection scheme responsive to the free tropospheric humidity simulate the cumulus congestus well. Compared with the somewhat similar total diabatic heating, stratiform heating differs substantially among the models. The cold bias in the upper troposphere in GAMIL and HIRAM is found to be related to the small convective mass flux and convective heating at upper levels in these two models. The evident connection between model systematic bias and model convective parameterization is a good justification of the CAPT approach. Overall, the varying types of convection and precipitation, from organized convection in the wet period, shallow convection in the dry period to the localized convection and organized squall lines in the break period, provide a vigorous test of the responsiveness of model physical schemes to different environmental conditions.

[30] Resolution impacts on model cloud properties are relatively minor when compared with the differences across the models driven, we speculate, by the different cloud and convective schemes. Model precipitation partitioning between L-S and convective is modulated by resolution with an overall increase of L-S precipitation with increased resolution. Resolution does not necessarily improve model systematic biases. In the break period over the coastal and inland region near Darwin, model convective precipitation possesses a clear diurnal cycle peaking from noon to late afternoon. As resolution increases, model L-S precipitation generally increases with a peak at night and thus modifies the total precipitation diurnal cycle in some models. In this sense, the model precipitation diurnal cycle can be significantly modulated by resolution, in addition to convective parameterizations.

[31] In depth investigation is needed to better understand model-specific performance and the connection between model characteristics and physics for each individual model. Nevertheless, the study emphasizes the importance of more environmentally responsive convective parameterizations to capture various types of convection as well as the substantial diversity among cloud and precipitation schemes in current AGCMs. The distinct types of tropical convection observed during the TWP-ICE provide a vigorous and useful test of model convective parameterizations and cloud schemes. Along with other coordinated intercomparisons, this case is an attractive test case for global atmospheric models.

[32] **Acknowledgments.** The authors thank the three anonymous referees for their constructive comments that helped to clarify and improve the paper. This research is supported by the Office of Science (BER), U.S. Department of Energy (Lin). TWP-ICE data were obtained from the ARM Program archive, sponsored by the DOE Office of Science, Office of Biological and Environmental Research, Environmental Science Division. The ECMWF analyses were provided to the ACRF data archive under a site license agreement. Support for J. Boyle, S. A. Klein and S. Xie was provided by the Atmospheric System Research and Regional and Global Climate Modeling Programs of the Office of Science at the U. S. Department of Energy. Their contribution to this work was performed

under the auspices of the U.S. Department of Energy by Lawrence Livermore National Laboratory under contract DE-AC52-07NA27344.

References

Ackerman, T. P., and G. Stokes (2003), The atmospheric radiation measurement program, *Phys. Today*, *56*, 38–45, doi:10.1063/1.1554135.

Bechtold, P., E. Bazile, F. Guichard, P. Mascart, and E. Richard (2001), A mass-flux convection scheme for regional and global models, *Q. J. R. Meteorol. Soc.*, *127*, 869–886, doi:10.1002/qj.49712757309.

Bechtold, P., J.-P. Chaboureau, A. Beljaars, A. K. Betts, M. Köhler, M. Miller, and J.-L. Redelsperger (2004), The simulation of the diurnal cycle of convective precipitation over land in global models, *Q. J. R. Meteorol. Soc.*, *130*, 3119–3137, doi:10.1256/qj.03.103.

Bechtold, P., M. Koehler, T. Jung, F. Doblas-Reyes, M. Leutbecher, M. J. Rodwell, F. Vitart, and G. Balsamo (2008), Advances in simulating atmospheric variability with the ECMWF model: From synoptic to decadal time-scales, *Q. J. R. Meteorol. Soc.*, *134*, 1337–1351, doi:10.1002/qj.289.

Betts, A., and C. Jakob (2002), Study of diurnal cycle of convective precipitation over Amazonia using a single column model, *J. Geophys. Res.*, *107*(D23), 4732, doi:10.1029/2002JD002264.

Boyle, J., and S. A. Klein (2010), Impact of horizontal resolution on climate model forecasts of tropical precipitation and diabatic heating for the TWP-ICE period, *J. Geophys. Res.*, *115*, D23113, doi:10.1029/2010JD014262.

Boyle, J. S., D. Williamson, R. Cederwall, M. Fiorino, J. J. Hnilo, J. G. Olson, T. Phillips, G. Potter, and S. Xie (2005), Diagnosis of Community Atmospheric Model 2 (CAM2) in numerical weather forecast configuration at Atmospheric Radiation Measurement sites, *J. Geophys. Res.*, *110*, D15S15, doi:10.1029/2004JD005042.

Boyle, J., S. Klein, G. Zhang, S. Xie, and X. Wei (2008), Climate model forecast experiments for TOGA COARE, *Mon. Weather Rev.*, *136*, 808–832, doi:10.1175/2007MWR2145.1.

Bretherton, C. S., J. R. McCaa, and H. Grenier (2004), A new parametrization for shallow cumulus convection and its application to marine subtropical cloud-topped boundary layers. Part I: Description and 1-D results, *Mon. Weather Rev.*, *132*, 864–882, doi:10.1175/1520-0493(2004)132<0864:ANPFSC>2.0.CO;2.

Dai, A., and K. E. Trenberth (2004), The diurnal cycle and its depiction in the Community Climate System Model, *J. Clim.*, *17*, 930–951, doi:10.1175/1520-0442(2004)017<0930:TDCAID>2.0.CO;2.

Deng, M., and G. G. Mace (2008), Cirrus cloud microphysical properties and air motion statistics using cloud radar Doppler moments: Water content, particle size, and sedimentation relationships, *Geophys. Res. Lett.*, *35*, L17808, doi:10.1029/2008GL035054.

Derbyshire, S. H., I. Beau, P. Bechtold, J.-Y. Grandpeix, J.-M. Piriou, J.-L. Redelsperger, and P. M. M. Soares (2004), Sensitivity of moist convection to environmental humidity, *Q. J. R. Meteorol. Soc.*, *130*, 3055–3079, doi:10.1256/qj.03.130.

Derbyshire, S. H., A. V. Maidens, S. F. Milton, R. A. Stratton, and M. R. Willett (2011), Adaptive detrainment in a convective parametrization, *Q. J. R. Meteorol. Soc.*, *137*, 1856–1871, doi:10.1002/qj.875.

de Rooy, W. C., and A. P. Siebesma (2010), Analytical expressions for entrainment and detrainment in cumulus convection, *Q. J. R. Meteorol. Soc.*, *136*, 1216–1227.

Dirmeyer, P. A., et al. (2012), Simulating the diurnal cycle of rainfall in global climate models: Resolution versus parameterization, *Clim. Dyn.*, doi:10.1007/s00382-011-1127-9, in press.

Donner, L. J. (1993), A cumulus parameterization including mass fluxes, vertical momentum dynamics, and mesoscale effects, *J. Atmos. Sci.*, *50*, 889–906, doi:10.1175/1520-0469(1993)050<0889:ACPIMF>2.0.CO;2.

Donner, L. J., C. J. Seman, R. S. Hemler, and S. Fan (2001), A cumulus parameterization including mass fluxes, convective vertical velocities, and mesoscale effects: Thermodynamic and hydrological aspects in a general circulation model, *J. Clim.*, *14*, 3444–3463, doi:10.1175/1520-0442(2001)014<3444:ACPIMF>2.0.CO;2.

Donner, L. J., et al. (2011), The dynamical core, physical parameterizations, and basic simulation characteristics of the atmospheric component of the GFDL Global Coupled Model CM3, *J. Clim.*, *24*, 3484–3519, doi:10.1175/2011JCLI3955.1.

Fridlind, A., et al. (2012), A comparison of TWP-ICE data with cloud-resolving model results, *J. Geophys. Res.*, *117*, D05204, doi:10.1029/2011JD016595.

Gent, P. R., et al. (2011), The Community Climate System Model Version 4, *J. Clim.*, *24*, 4973–4991, doi:10.1175/2011JCLI4083.1.

GFDL Global Atmospheric Model Development Team (2004), The new GFDL global atmosphere and land model AM2–LM2: Evaluation with prescribed SST simulations, *J. Clim.*, *17*, 4641–4673, doi:10.1175/JCLI-3223.1.

Gregory, D., and P. R. Rowntree (1990), A mass flux convection scheme with representation of cloud ensemble characteristics and stability-dependent closure, *Mon. Weather Rev.*, *118*, 1483–1506, doi:10.1175/1520-0493(1990)118<1483:AMFCSW>2.0.CO;2.

Gregory, D. R., R. Kershaw, and P. M. Inness (1997), Parameterization of momentum transport by convection: II. Tests in single-column and general circulation models, *Q. J. R. Meteorol. Soc.*, *123*, 1153–1183, doi:10.1002/qj.49712354103.

Hack, J. J. (1994), Parameterization of moist convection in the National Center for Atmospheric Research Community Climate Model (CCM2), *J. Geophys. Res.*, *99*(D3), 5551–5568, doi:10.1029/93JD03478.

Heymsfield, A., et al. (2008), Testing IWC retrieval methods using radar and ancillary measurements with in situ data, *J. Appl. Meteorol. Climatol.*, *47*, 135–163, doi:10.1175/2007JAMC1606.1.

Huffman, G. J., R. F. Adler, D. T. Bolvin, G. Gu, E. J. Nelkin, K. P. Bowman, Y. Hong, E. F. Stocker, and D. B. Wolff (2007), The TRMM multisatellite precipitation analysis (TMPA): Quasi-global, multiyear, combined-sensor precipitation estimates at fine scales, *J. Hydrometeorol.*, *8*(1), 38–55, doi:10.1175/JHM560.1.

Japan Meteorological Agency (2007), Outline of the Operational Forecast and Analysis System of the Japan Meteorological Agency (March 2007), report, Tokyo. [Available at http://www.jma.go.jp/jma/jma-eng/jma-center/nwp/outline-nwp/index.htm.]

Jung, T., S. K. Gulev, I. Rudeva, and V. Soloviov (2006), Sensitivity of extratropical cyclone characteristics to horizontal resolution in the ECMWF model, *Q. J. R. Meteorol. Soc.*, *132*, 1839–1857.

Jung, T., G. Balsamo, P. Bechtold, A. C. M. Beljaars, M. Köhler, M. J. Miller, J.-J. Morcrette, A. Orr, M. J. Rodwell, and A. M. Tompkins (2010), The ECMWF model climate: Recent progress through improved physical parametrizations, *Q. J. R. Meteorol. Soc.*, *136*, 1145–1160.

Kim, D., A. H. Sobel, E. D. Maloney, D. M. W. Frierson, and I.-S. Kang (2011), A systematic relationship between intraseasonal variability and mean state bias in AGCM simulations, *J. Clim.*, *24*, 5506–5520, doi:10.1175/2011JCLI4177.1.

Lau, N.-C., and J. J. Ploshay (2009), Simulation of synoptic- and subsynoptic-scale phenomena associated with the East Asian summer monsoon using a high-resolution GCM, *Mon. Weather Rev.*, *137*(1), 137–160, doi:10.1175/2008MWR2511.1.

Lin, J., B. Mapes, M. Zhang, and M. Newman (2004), Stratiform precipitation, vertical heating profiles, and the Madden Julian oscillation, *J. Atmos. Sci.*, *61*(3), 296–309, doi:10.1175/1520-0469(2004)061<0296:SPVHPA>2.0.CO;2.

Lin, J.-L., et al. (2006), Tropical intraseasonal variability in 14 IPCC AR4 climate models: Part I. Convective signals, *J. Clim.*, *19*(12), 2665–2690, doi:10.1175/JCLI3735.1.

Majewski, D., et al. (2002), The operational global icosahedral–hexagonal gridpoint model GME: Description and high-resolution tests, *Mon. Weather Rev.*, *130*, 319–338, doi:10.1175/1520-0493(2002)130<0319:TOGIHG>2.0.CO;2.

Martin, G. M., M. A. Ringer, V. D. Pope, A. Jones, C. Dearden, and T. J. Hinton (2006), The physical properties of the atmosphere in the new Hadley Centre Global Environmental Model (HadGEM1). Part I: Model description and global climatology, *J. Clim.*, *19*, 1274–1301, doi:10.1175/JCLI3636.1.

Martin, G. M., S. F. Milton, C. A. Senior, M. E. Brooks, S. Ineson, T. Reichler, and J. Kim (2010), Analysis and reduction of systematic errors through a seamless approach to modeling weather and climate, *J. Clim.*, *23*, 5933–5957, doi:10.1175/2010JCLI3541.1.

May, P., and A. Ballinger (2007), The statistical characteristics of convective cells in a monsoon regime (Darwin, Northern Australia), *Mon. Weather Rev.*, *135*, 82–92, doi:10.1175/MWR3273.1.

May, P. T., J. H. Mather, G. Vaughan, C. Jakob, G. M. McFarquhar, K. N. Bower, and G. G. Mace (2008), The tropical warm pool international cloud experiment, *Bull. Am. Meteorol. Soc.*, *89*(5), 629–645, doi:10.1175/BAMS-89-5-629.

Ming, Y., V. Ramaswamy, L. J. Donner, and V. T. J. Phillips (2006), A new parameterization of cloud droplet activation applicable to general circulation models, *J. Atmos. Sci.*, *63*, 1348–1356, doi:http://dx.doi.org/10.1175/JAS3686.1.

Minnis, P., W. L. Smith Jr., D. F. Young, L. Nguyen, A. D. Rapp, P. W. Heck, S. Sun-Mack, Q. Trepte, and Y. Chen (2001), A near-real time method for deriving cloud and radiation properties from satellites for weather and climate studies, paper presented at 11th Conference on Satellite Meteorology and Oceanography, Am. Meteorol. Soc., Madison, Wis.

Moorthi, S., and M. J. Suarez (1992), Relaxed Arakawa-Schubert: A parameterization of moist convection for general circulation models, *Mon. Weather Rev.*, *120*, 978–1002, doi:10.1175/1520-0493(1992)120<0978:RASAPO>2.0.CO;2.

Morrison, H., and A. Gettelman (2008), A new two-moment bulk stratiform cloud microphysics scheme in the Community Atmosphere Model, version 3(CAM3). Part I: Description and numerical tests, *J. Clim.*, *21*, 3642–3659, doi:10.1175/2008JCLI2105.1.

Neale, R. B., J. H. Richter, and M. Jochum (2008), The impact of convection on ENSO: From a delayed oscillator to a series of events, *J. Clim.*, *21*(22), 5904–5924, doi:10.1175/2008JCLI2244.1.

Pan, D.-M., and D. A. Randall (1998), A cumulus parameterization with a prognostic closure, *Q. J. R. Meteorol. Soc.*, *124*, 949–981.

Petch, J. C., M. R. Willett, R. Y. Wong, and S. J. Woolnough (2007), Modelling suppressed and active convection: Comparing a numerical weather prediction, cloud-resolving and single-column model, *Q. J. R. Meteorol. Soc.*, *133*, 1087–1100, doi:10.1002/qj.109.

Phillips, T. J., et al. (2004), Evaluating parameterizations in general circulation models: Climate simulation meets weather prediction, *Bull. Am. Meteorol. Soc.*, *85*, 1903–1915, doi:10.1175/BAMS-85-12-1903.

Plant, R. S. (2010), A review of the theoretical basis for bulk mass flux convective parameterization, *Atmos. Chem. Phys.*, *10*, 3529–3544, doi:10.5194/acp-10-3529-2010.

Protat, A., J. Delanoe, D. Bouniol, A. Heymsfield, A. Bansemer, and P. Brown (2007), Evaluation of ice water content retrievals from cloud radar reflectivity and temperature using a large airborne in situ microphysical database, *J. Appl. Meteorol. Climatol.*, *46*, 557–572, doi:10.1175/JAM2488.1.

Randall, D. A., et al. (2007), Climate models and their evaluation, in *Climate Change 2007: The Physical Science Basis*, edited by S. Solomon et al., pp. 589–662, Cambridge Univ. Press, Cambridge, U. K.

Rasch, P. J., and J. E. Kristjansson (1998), A comparison of the CCM3 model climate using diagnosed and predicted condensate parameterizations, *J. Clim.*, *11*, 1587–1614, doi:10.1175/1520-0442(1998)011<1587:ACOTCM>2.0.CO;2.

Rodwell, M. J., and T. N. Palmer (2007), Using numerical weather prediction to assess climate models, *Q. J. R. Meteorol. Soc.*, *133*, 129–146, doi:10.1002/qj.23.

Rotstayn, L. D. (1997), A physically based scheme for the treatment of stratiform clouds and precipitation in large-scale models. I: Description and evaluation of the microphysical processes, *Q. J. R. Meteorol. Soc.*, *123*, 1227–1282.

Rutledge, S. A., and P. Hobbs (1983), The mesoscale and microscale structure and organization of clouds and precipitation in midlatitude cyclones. VIII: A model for the "seeder-feeder" process in warm-frontal rainbands, *J. Atmos. Sci.*, *40*, 1185–1206, doi:10.1175/1520-0469(1983)040<1185:TMAMSA>2.0.CO;2.

Smith, R. N. B. (1990), A scheme for predicting layer clouds and their water content in a general circulation model, *Q. J. R. Meteorol. Soc.*, *116*, 435–460, doi:10.1002/qj.49711649210.

Sundqvist, H., E. Berge, and J. E. Kristjánsson (1989), Condensation and cloud parameterization studies with a mesoscale numerical weather prediction model, *Mon. Weather Rev.*, *117*, 1641–1657, doi:10.1175/1520-0493(1989)117<1641:CACPSW>2.0.CO;2.

Tiedtke, M. (1989), A comprehensive mass flux scheme for cumulus parameterization in large-scale models, *Mon. Weather Rev.*, *117*, 1779–1800, doi:10.1175/1520-0493(1989)117<1779:ACMFSF>2.0.CO;2.

Tiedtke, M. (1993), Representation of clouds in large-scale models, *Mon. Weather Rev.*, *121*, 3040–3061, doi:10.1175/1520-0493(1993)121<3040:ROCILS>2.0.CO;2.

Tompkins, A. M. (2002), A prognostic parameterization for the subgrid-scale variability of water vapor and clouds in large-scale models and its use to diagnose cloud cover, *J. Atmos. Sci.*, *59*, 1917–1942, doi:10.1175/1520-0469(2002)059<1917:APPFTS>2.0.CO;2.

Turner, D. D., S. A. Clough, J. C. Liljegren, E. E. Clothiaux, K. Cady-Pereira, and K. L. Gaustad (2007), Retrieving liquid water path and precipitable water vapor from Atmospheric Radiation Measurement (ARM) microwave radiometers, *IEEE Trans. Geosci. Remote Sens.*, *45*(11), 3680–3690, doi:10.1109/TGRS.2007.903703.

Waliser, D. E., et al. (2009), Cloud ice: A climate model challenge with signs and expectations of progress, *J. Geophys. Res.*, *114*, D00A21, doi:10.1029/2008JD010015.

Wapler, K., and T. P. Lane (2011), A case of offshore convective initiation by interacting land breezes near Darwin, Australia, *Meteorol. Atmos. Phys.*, *115*, 123–137, doi:10.1007/s00703-011-0180-6.

Willett, M. R., P. Bechtold, D. L. Williamson, J. C. Petch, S. F. Milton, and S. J. Woolnough (2008), Modeling suppressed and active convection: Comparisons between three global atmospheric models, *Q. J. R. Meteorol. Soc.*, *134*, 1881–1896, doi:10.1002/qj.317.

Williamson, D. L., and J. G. Olson (2007), A comparison of forecast errors in CAM2 and CAM3 at the ARM Southern Great Plains Site, *J. Clim.*, *20*, 4572–4585, doi:10.1175/JCLI4267.1.

Williamson, D. L., J. Boyle, R. Cederwall, M. Fiorino, J. Hnilo, J. Olson, T. Phillips, G. Potter, and S. C. Xie (2005), Moisture and temperature balances at the ARM Southern Great Plains Site in forecasts with the CAM2, *J. Geophys. Res.*, *110*, D15S16, doi:10.1029/2004JD005109.

Wilson, D. R., and S. P. Ballard (1999), A microphysically based precipitation scheme for the UK Meteorological Office unified model, *Q. J. R. Meteorol. Soc.*, *125*, 1607–1636, doi:10.1002/qj.49712555707.

Xie, S., J. Boyle, S. A. Klein, X. Liu, and S. Ghan (2008), Simulations of Arctic mixed-phase clouds in forecasts with CAM3 and AM2 for M-PACE, *J. Geophys. Res.*, *113*, D04211, doi:10.1029/2007JD009225.

Xie, S., T. Hume, C. Jakob, S. A. Klein, R. B. McCoy, and M. Zhang (2010), Observed large-scale structures and diabatic heating and drying profiles during TWP-ICE, *J. Clim.*, *23*(1), 57–79, doi:10.1175/2009JCLI3071.1.

Yanai, S., M. Esbensen, and J.-H. Chu (1973), Determination of bulk properties of tropical cloud clusters from large-scale heat and moisture budgets, *J. Atmos. Sci.*, *30*, 611–627, doi:10.1175/1520-0469(1973)030<0611:DOBPOT>2.0.CO;2.

Yang, G.-Y., and J. Slingo (2001), The diurnal cycle in the tropics, *Mon. Weather Rev.*, *129*, 784–801, doi:10.1175/1520-0493(2001)129<0784:TDCITT>2.0.CO;2.

Zhang, G. J., and N. A. McFarlane (1995), Sensitivity of climate simulations to the parameterization of cumulus convection in the Canadian Climate Centre general circulation model, *Atmos. Ocean*, *33*, 407–446, doi:10.1080/07055900.1995.9649539.

Zhang, M., W. Lin, C. S. Bretherton, J. J. Hack, and P. J. Rasch (2003), A modified formulation of fractional stratiform condensation rate in the NCAR Community Atmospheric Model (CAM2), *J. Geophys. Res.*, *108*(D1), 4035, doi:10.1029/2002JD002523.

Zhao, C., et al. (2012), Toward understanding of differences in current cloud retrievals of ARM ground-based measurements, *J. Geophys. Res.*, doi:10.1029/2011JD016792, in press.

Zhao, M., I. M. Held, S.-J. Lin, and G. A. Vecchi (2009), Simulations of global hurricane climatology, interannual variability, and response to global warming using a 50 km resolution GCM, *J. Clim.*, *22*(24), 6653–6678, doi:10.1175/2009JCLI3049.1.